Effect of spin transfer torque on domain wall motion regimes in [Co/Ni] superlattice wires

S. Le Gall, N. Vernier, F. Montaigne, A. Thiaville, J. Sampaio, D. Ravelosona, S. Mangin, S. Andrieu, and T. Hauet

Effect of spin transfer torque on domain wall motion regimes in [Co/Ni] superlattice wires

S. Le Gall[1,2*], N. Vernier[3], F. Montaigne[1], A. Thiaville[4], J. Sampaio[4], D. Ravelosona[3], S. Mangin[1], S. Andrieu[1] and T. Hauet[1]

[1]Institut Jean-Lamour, UMR 7198, CNRS, Univ. Lorraine, Nancy, France
[2]Génie Electrique et Electronique de Paris, UMR 8507, CNRS, CentraleSupelec, Univ. Paris-Sud, UPMC, 11 rue Joliot Curie, Plateau de Moulon, Gif-sur-Yvette, France
[3]Institut d'Electronique Fondamentale, UMR 8622, CNRS, Univ. Paris-Sud, Orsay, France
[4]Laboratoire de Physique des Solides, UMR 8502, CNRS, Univ. Paris-Sud, Orsay, France

The combined effect of magnetic field and current on domain wall motion is investigated in epitaxial [Co/Ni] microwires. Both thermally activated and flow regimes are found to be strongly affected by current. All experimental data can be understood by taking into account both adiabatic and non-adiabatic components of the spin transfer torque, parameters of which are extracted. In the precessional flow regime, it is shown that the domain wall can move in the electron flow direction against a strong applied field, as previously observed. In addition, for a large range of applied magnetic field and injected current, a stochastic domain wall displacement after each pulse is observed. Two-dimensional micromagnetic simulations including some disorder show a random fluctuation of the domain wall position, that qualitatively matches the experimental results.

* sylvain.le-gall@u-psud.fr

The manipulation of magnetization by spin-transfer torque (STT) [1, 2] shows promise for the development of new data storage electronic devices. For instance, current-induced domain wall motion [3] may be implemented to increase the density, performance and endurance of non-volatile storage devices [4]. Materials with out-of-plane anisotropy are promising candidates [5-7], as they can host narrow domain walls (DW), which are attractive for maximizing storage density and improving current-induced domain wall displacement efficiency. [Co/Ni] superlattices are often considered as an promising material for nanostructured spintronic devices because of their tunable magnetic and spin-electronic properties [5, 8, 9], especially for domain wall motion by STT [10-12]. However, in sputtered [Co/Ni] systems, specifically nanowires based on perpendicular anisotropy films, the current-induced DW motion has usually been studied in a restricted velocity regime. As a result, the adiabatic and non-adiabatic STT terms have been determined separately: Burrowes *et al.* [11] found that the non-adiabatic torque dominates the DW depinning and creep motion, whereas Koyama *et al.* [12] found the opposite, in the flow regime.

In this work, in order to extend the understanding of the effect of STT on DW motion, we propose a complete study in both velocity regimes, namely thermally activated and precessional flow. The sample used is a well-controlled [Co/Ni] superlattice with strong perpendicular magnetic anisotropy (PMA) grown by molecular beam epitaxy (MBE) [13-15]. We have studied the current and field-

induced DW motion using Kerr magneto-optical microscopy. We demonstrate that the current has a strong impact on the two velocity regimes. The evolution of the DW velocity under combined pulsed field and current excitation is understood by taking into account both adiabatic and non-adiabatic components of STT [16, 17]. For small fields, the parameters necessary to describe this behavior are extracted considering an Arrhenius law modified by STT. For large fields, the measured DW velocities in the precessional flow regime are consistent with the one-dimensional model for DW motion [18]. The extracted parameters explain the experimental data over the entire range of fields studied. We find that the DW can move in the electron flow direction against the external magnetic field, even for an amplitude as high as 20 mT, as previously observed [19]. Finally, for large current densities opposing the magnetic field effect, the DW motion direction is observed to be stochastic. Micromagnetic simulations including the presence of disorder reproduce this feature qualitatively.

The samples were grown epitaxially on a sapphire substrate using MBE [13, 15] under ultra-high vacuum. The superlattice stack consists of : Al_2O_3/V(5)/Au(1)/Ni(0.2)/[Co(0.5)/Ni(0.6)]$_{\times 3}$ /Au(1.2), with thicknesses in nanometers. The crystallinity and the layer-by-layer growth were monitored during deposition by recording RHEED patterns and their intensity oscillation. Using a SQUID-VSM magnetometer, the following parameters were determined: saturation magnetization $M_S = 9.3 \times 10^5$ A/m (930 emu/cm^3), effective anisotropy $K_{eff} = 3.0 \times 10^5$ J/m^3 (3.0×10^4 erg/cm^3), and uniaxial magnetocrystalline anisotropy $K_U = 8.4 \times 10^5$ J/m^3 (8.4×10^4 erg/cm^3) [14]. Gold was used as capping and seed layer of the stack to avoid the spin-orbit torque observed in ferromagnetic nanowires with structural inversion asymmetry [20, 21]. In order to study the current-induced DW motion, the sample was patterned into micron-wide wires (2-10 μm) by UV lithography and dry etching. An optical view of a 2 μm-wide wire is shown in Fig. 1(a). The 90 μm-long magnetic wire consists of 2 Hall crosses (not used in these experiments) and terminates in a triangular-shape large pad for DW nucleation. Non-magnetic contacts are patterned on each wire end, for electrical current injection. The DW displacement is observed and quantified using magneto-optical Kerr effect (MOKE) microscopy. The magnetic configurations were imaged using a 25× magnification Leitz lens with 0.22 numerical aperture which gives a nominal resolution around 1 μm. All experiments were done at room temperature (RT).

To quantify the current-induced DW motion, it is necessary to inject a high current density to observe a significant effect. The use of μs-pulsed current (I_{pulse}) excitation alone is not enough to move the DW in the wire by STT; a pulsed magnetic field is also required. Using both field and current, the impact of STT on DW motion could be observed and analyzed. In our experiments, a home-made coil was used to apply μs-pulsed magnetic fields (H_{pulse}) homogeneously over the sample. In order to quantify the DW displacement, combined H_{pulse} and I_{pulse} excitations were synchronized. Due to the finite coil rise-time, the I_{pulse} trigger is delayed by 2 μs after the H_{pulse} trigger. For all experiments, the synchronized pulse durations were 5 μs for H_{pulse} and 3 μs for I_{pulse}, with a 2 μs delay (see Fig. 1(b)). During the 2 μs magnetic field rise time, the applied magnetic field has a small impact on DW motion. The amplitude of each pulse was controlled using an oscilloscope (Fig. 1(b)).

The study of current and field-induced DW motion was done on a single wire with 2 μm width. A sequence of DW displacements is shown on Fig. 1(c) for $J_{pulse} = +21 \times 10^{10}$ A/m² and $\mu_0 H_{pulse} = 20.5$ mT. The DW nucleation takes place on the right large pad, and the DW is injected in the wire by the right side using a low H_{pulse}. The upper picture in Fig. 1(c) shows the DW position at the entrance of the wire. Each subsequent frame shows, by image difference, the DW displacement after one single pulse. In this manner, we can measure the DW displacement after each pulse. The average DW velocity is

calculated by dividing the displacement by the pulse duration (3 µs). When the DW displacement after a single pulse is too small to be observed, a series of pulses (up to 50) is used instead, so as to observe a significant displacement. Since DW injection into the wire always occurs from the pad, by the current sign convention implies that a negative current is expected to favor by STT, field-driven DW propagation, whereas a positive current induces a STT which opposes the field-driven motion.

Measured DW velocities for various H_{pulse} and $\pm J_{pulse}$ amplitudes are plotted in Fig. 2 in semi-logarithmic scale. Figure 2(a), resp. 2(b) shows negative, resp. positive current densities. The black cross symbol curve plotted on both figures represents the field-induced DW motion at zero current, as a reference for the two graphs. This curve is similar to that obtained for the full film [15], where two velocity regimes are observed. The first one, at low field, is a thermally activated regime (Arrhenius-type) described by $v(H)=v_0 \exp[2M_S V_a(H-H_{dep})/k_B T]$ where v_0 is the prefactor, and H_{dep} the depinning field (above which the DW leaves this regime) [22]. The second one, at larger fields, is a flow regime where the velocity saturates around 10 m/s [15, 23]. The depinning field is around 21 mT at zero current, slightly lower than observed previously on the full film (24 mT [15]), possibly due to the effect of patterning. In Fig. 2, most of the data correspond to the transition between thermally activated and flow regimes [15], except in the high positive current case where the magnetic field and the current seem to have no effect on the DW motion [24]. We will treat this unusual regime later separately. In the following, we show that two independent models, characteristic of the thermally activated regime for the first one and the flow regime for the second one, can explain our experimental data using a single set of parameters. The specific regime observed for $J_{pulse} > 21 \times 10^{10}$ A.m^{-2} will be analyzed at the end of the paper.

To obtain a better understanding on how the thermally activated regime is affected by the injected current, the DW velocities only in this regime are plotted on Fig. 3(a) for both positive and negative J_{pulse}. For $J_{pulse}<0$, the curves shift significantly downfield as compared to the zero-current curve (black crosses), i.e. for a given field, DW velocity increases with the amplitude of negative current. Thus, negative currents facilitate DW displacement as expected for STT. On the other hand, for $J_{pulse}>0$, no strong effect of the current is observed in Fig. 3(a). Moreover, whereas a decrease of DW velocity with respect to zero current would be expected for positive current, the DW velocity is larger for $J_{pulse} = + 21 \times 10^{10}$ A/m². In order to quantify the effect of current in the thermally activated regime, we introduce an effective field ΔH, the field shift with respect to zero-current velocity curve (taken as reference). The field shift ΔH is measured as follows: for each $J_{pulse} \neq 0$, we measure a series of field shifts for varying values of $\mu_0 H$; the ΔH associated to that current density is their mean and the accuracy is their standard deviation. An example of field shift (red arrow) is displayed in the inset of Fig. 3(b) for the velocity at $J=-9 \times 10^{10}$ A/m² at $\mu_0 H=17.5$ mT. The field shift ΔH is counted positive for a shift to the left with respect to the zero-current velocity curve. In Fig. 3(b), we present the extracted ΔH values versus J_{pulse} with the error bars. The experimental points can be fitted by a second-degree polynomial (red line): $\Delta H = +\varepsilon J_{pulse} + \eta J_{pulse}^2$ with $\varepsilon=-(6.3\pm0.9)\times10^{-15}$ T/A.m^{-2} and $\eta=(3.3\pm0.3)\times10^{-26}$ T/A².m^{-4}. It is equivalent to consider that the Arrhenius law can be rewritten as $v(H)=v_0\exp[2M_S V_a(H_{eff}-H_{dep})/k_B T]$, where $H_{eff} = H_{pulse} + \varepsilon J_{pulse} + \eta J_{pulse}^2$ is an effective out-of-plane field.

For the physical origin of such a J dependence, we refer to Ref. [25], a theoretical analysis of the current-induced DW motion by magnetic field in the creep regime including both non-adiabatic and adiabatic components of STT. A non-adiabatic term proportional to the current (εJ) that acts as a magnetic field [26], and a quadratic adiabatic term (ηJ^2) which introduces non-linearity to H, are added

to the velocity expression in the creep regime. This theory was successfully used to interpret the experimental observation of the DW motion in GaMnAs nanowires [27, 28]. From the efficiency ε, we can deduce β, the so-called non-adiabaticity STT constant, since $|\varepsilon| = (\beta P \hbar)/(2eM_S\Delta)$ [26], where P is the spin polarization (P=0.56 being estimated in the flow regime, see below), and Δ=5.8 nm the DW thickness [29]. We obtain β=(0.18±0.02), a value around 8 times bigger than reported on sputtered [Co/Ni] system in the creep regime [11]. For sputtered [Co/Ni] systems, the relative contribution of both adiabatic and non-adiabatic terms is still unclear: Burrowes *et al.* [11] found that the non-adiabatic torque dominates the DW creep motion and depinning, whereas Koyama *et al.* [12] found that it plays no significant role. If we base our analysis on the theoretical expression from [25], we find that both adiabatic and non-adiabatic components may play a significant role on DW propagation in the thermally-activated regime in epitaxial [Co/Ni] samples. The sign of the quadratic term (ηJ^2) can be positive or negative according to equation (1) of reference [28]. The J^2 dependence could also relate to Joule heating. We use the following estimation of the temperature rise ΔT coming from Joule heating by a current pulse [30] $\Delta T = RI^2 \times (\ln(16K/(dCw^2)) + \ln(\tau_{pulse}))/(2\pi lK)$, which depends on C, K and d, the specific heat, thermal conduction, and density of the substrate respectively, the resistivity R and dimensions (l, w) of the wire, and pulse duration τ_{pulse}. Taking d=4000 kg/m^3, K=40 W.m^{-1}.K^{-1}, C=700 J.kg^{-1}.K^{-1} for sapphire and R=1500 Ω, w=2 μm and l=165 μm for our Co/Ni layer, one calculates that an injected current between 20 and 45×10^{10} A/m^2 in our microwire gives rise to a slight temperature increase of about 4 – 20 K . The Joule heating contributes to an increase of temperature by $T+\delta J^2$ with δ a constant. This affects the slope of the v(J) curve in the thermally activated regime, because it decreases the potential energy barrier in the Arrhenius law. Therefore Joule heating does not cause the strong shift of the curves toward positive current that is observed.

As a first analysis of the data in the flow regime, we use the one-dimensional model with disorder proposed by Tatara *et al.* [18]. In this model, the DW configuration, moved by external field and current, is described by simply 2 coordinates: the DW position X and the tilting angle Φ that the DW magnetization forms with the easy axis plane. The following equations hold:

$$\begin{cases} \dot{\Phi} + \alpha\dot{X}/\Delta = \gamma H + \beta u/\Delta + f_{pin} \\ \dot{X} - \alpha\Delta\dot{\Phi} = v_\perp \sin 2\Phi + u \end{cases} \tag{1}$$

where H is the external magnetic field, α the damping parameter, β the nonadiabaticity parameter of the STT, γ the gyromagnetic ratio (1.8×10^{11} Hz/T for [Co/Ni] [31]), Δ the DW width, f_{pin} the pinning force and $v\perp$ is a velocity related to the hard-axis magnetic anisotropy (also known as the Walker velocity). The last parameter $u=gP\mu_B J/(2eM_S)$ is a term proportional to the current density J which is equivalent to a velocity (sometimes called the spin drift velocity). Here g=2.0 is the Landé factor, P the spin polarization, μ_B the Bohr magneton, and M_S the saturation magnetization. The DW velocity at long times is the time-average $v = <\dot{X}>$ after depinning (f_{pin}=0). Using the same method provided in the supplementary materials from Ref. [19], we deduce that the DW velocity can be expressed in the flow regime as the following sum:

$$v = v_H + v_J \tag{2}$$

where v_H and v_J are respectively the field and current contribution given by:

$$v_H = \frac{\Delta\gamma H}{\alpha}\left(1 - \frac{1}{1+\alpha^2}\sqrt{1 - \left(\frac{H_W}{H}\right)^2}\right) \tag{3}$$

$$v_J = \frac{\beta}{\alpha}u + \frac{u}{1+\alpha^2}\left(1-\frac{\beta}{\alpha}\right)\sqrt{1-\left(\frac{H_W}{H}\right)^2} \qquad (4)$$

where H_w is the Walker breakdown field. Equations (2), (3) and (4) allow the interpretation of our experimental data in the flow regime.

To get a better view of the impact of STT on the DW motion in the flow regime, the velocities in this regime are replotted in Fig. 3(c). For zero-current, the velocity saturates at 13 m/s, so v_H is constant as seen before in the case where the damping is very small [19]. Under field and current, we notice that the saturated velocity increases as the current density decreases, consistent with Eq. (2). Using this equation, we quantify v_J. Note that, for our Co/Ni system, we can simplify the v_J expression [19]. Indeed, the damping parameter was measured to $\alpha \approx 0.02$ by ferromagnetic resonance (see also reference [31]) which leads to $\mu_0 H_w \approx 1.5$ mT. Thus, in the precessional flow regime, we have $\alpha^2 \ll 1$ and $H_w \ll H$, so that v_J in Eq.(4) can be approximated to [19]:

$$v_J = u = \frac{gP\mu_B}{2eM_S}J \qquad (5)$$

The processing of experimental data in the precessional flow regime in Fig 3(c) should be made in the region where the velocity saturates (plateau). For $|J_{pulse}| < 9 \times 10^{10}$ A/m², this regime appears for strong fields ($\mu_0 H_{pulse} > 22$ mT), whereas outside this range, it appears at lower fields. To determine v_J from the experimental data, we used the following method: the difference Δv between saturated velocity for the same opposite current density should give $2 \times v_J$. For each opposite current, we measure a series of Δv for various $\mu_0 H_{pulse}$, the mean giving $2 \times v_J$ and the standard deviation being the accuracy. The inset of Fig. 3(d) shows the method for extracting Δv for $J_{pulse} = 9 \times 10^{10}$ A/m² at $\mu_0 H_{pulse} = 24$ mT.

The current contribution to the velocity v_J, is plotted as a function of current density in Fig. 3(d). We find that v_J is proportional to J, in agreement with Eq. (5). The slope gives $v_J/J_{pulse} = (3.6 \pm 0.3) \times 10^{-11}$ m³.A⁻¹.s⁻¹, corresponding to a spin-polarization $P = 0.56 \pm 0.05$ (0.65 ± 0.1 was measured by spin-resolved photoemission spectroscopy [32] for the same stack). Using magneto-transport measurements, a spin-polarization in the range $0.5 - 0.8$ at 300 K (for instance see Ref. [19, 33-34]) was reported in the literature for sputtered-growth [Co/Ni] multi-layers due to thickness of both Co and Ni layers and stack number dependence [34]. These results confirm that the expressions of the above 1D model are suitable for our system. Therefore, the experimental behavior of velocities observed in Fig. 2 can be explained in a large field range by a set of parameters found in the two independent regimes. This gives credit to our quantification of the non-adiabatic and adiabatic STT terms in [Co/Ni].

Next, we focus on the high field case with positive current densities, where v_H and v_J are in opposite directions. DW displacement against the magnetic field at high current density has already been observed on sputtered [Co/Ni] nanowires, and is more generally predicted for materials with low damping constant α [19]. This effect occurs in the precessional regime where the DW is depinned by H but where v_H is small so that DW propagation is dominated by the current. According to Eq. (2) v_J should dominate (J-driven DW motion case) for $v_J > 13$ m/s since v_H saturates at 13 m/s for large field (see Fig. 2(a)). Such behavior is experimentally observed for J_{pulse} close to $+25 \times 10^{10}$ A/m² as calculated with Eq. (5). Nevertheless, we observed that, for the same injected current, the domain wall moves stochastically either in the direction favored by the magnetic field (Fig. 4(a)) or against it (Fig.

4(b)). As an example, in Fig. 4(a) and 4(b), we present the results of two successive experiments performed in the same conditions with $\mu_0 H_{pulse}$=25 mT and J_{pulse}= +33×10^{10} A/m². Displacements of a few micrometers for single pulses lead to unambiguous results about the direction of DW motion. Note that the structural symmetry of our system and the use of Au for the capping and seed layers are expected to suppress spin-orbit torques [20, 21]. We note that due to sample design, Koyama *et al.* [19], could observe DW motion only in one direction of propagation, so could not detect the stochastic phenomena evidenced here.

This stochasticity extends over a large current density range, at least up to +45×10^{10} A/m². Figure 4(c) shows all experimental displacements measured for $J_{pulse} \geq$ +33×10^{10} A/m². We have assigned positives values for DW displacement in the H-field direction (Fig. 4(a)), and negative ones for DW displacement against it (Fig. 4(b)). Zero displacements are also observed, meaning that sometimes the DW is pinned or the displacement is smaller than the optical resolution of 1 μm. Small displacements can also take place by auto-motion, where a structural change of the DW by STT leads to a DW displacement by itself [35], an effect also called DW inertia [36]. For [Co/Ni], using the DW width and damping quoted above, this auto-motion is estimated around 1 μm. The blue shaded regions displayed in Fig. 4(c) indicate the range where auto-motion could occur and/or no DW motion by pinning.

The displacements displayed for various H_{pulse} and J_{pulse} in Fig. 4(c) form clouds meaning that DW velocity is quasi-independent of J_{pulse}. This result is unexpected according to the expression of v_J at long times. The statistical distribution of the set of DW displacements is shown in Fig 4(d) without taking into account the value of the injected current density. This distribution is bell-shaped, with a slight skew asymmetry. The presence of a peak centered at zero is in favor of a random walk mechanism with compensation when v_H+v_J=0. Note that the asymmetry may be a statistical artifact due to the small sample number of events (120 in total).

According to Eq. (5), v_J is proportional to J_{pulse}, so that v_H+v_J=0 should no longer hold for higher J_{pulse}. For instance taking J_{pulse} =+45×10^{10} A/m², according to the slope v_J/J_{pulse}= (3.6±0.3)×10^{-11} m^3.A^{-1}.s^{-1} deduced from Fig. 3(d), v_J should reach (16.2±1.4) m/s, leading to a velocity around v= (-7±1.5) m/s. At this value, the DW should move against field, not in the thermally activated regime. However, we measure (Fig. 2(b)) a DW velocity around +/- 2 m/s. The DW motion is therefore slower than expected, which corresponds to the observed stochasticity and pinning. Thus, if we come back to the previous Fig. 2(b) depicting the complete v(H) curves for positives J_{pulse} (by keeping H-driven case only), we attribute the strong change of the v(H) characteristic for $J_{pulse} \geq$ +33×10^{10} A/m² to the stochasticity. The decrease of the velocity for high current density cannot be explained using Eq. (5) unless we consider a huge drop of spin-polarization (not consistent with the expected temperature dependence of P [33] due to the increase of temperature (max 20 K) coming from Joule heating produced by current pulse). Thus, the 1D model is insufficient to describe the DW velocities in the stochastic regime. Investigation of current-induced DW motion in the nanosecond timescale [37] might reveal ultra-fast back-and-forth movements of the DW.

To study the physics of this stochastic behaviour, we have performed 2D micromagnetic simulations of propagating DWs under field and current in a 1 μm-wide and 3.5 nm-thick track using the Mumax3 code [38]. The simulation parameters were: cell lateral size 2 nm, damping factor 0.02, exchange stiffness 10 pJ/m, anisotropy constant K_U=8.4×10^5 J/m^3, and saturation magnetization M_S=9.3×10^5 A/m. To emulate the pinning induced by a variability in film thickness, we have divided the system into grains of random shape (mean diameter of 15 nm) of different anisotropy parameter

K_U and saturation magnetization M_S (see Fig. 5(b)). The disorder model stemming from an assumed variation of thickness, the values of M_S and $1/K_U$ are assumed to follow a Gaussian distribution, with a standard deviation of 3% chosen so that the depinning field matches the experiments. For each set of magnetic field and current density values, we have repeated the simulation with different initial states: a homogenous Bloch wall pointing either up or down and "randomized" DWs containing sections pointing up or down with Bloch lines in between. The latter walls were prepared by submitting the homogeneous DWs to an intense easy-axis field for 1 ns. In all studied cases, the DW magnetization precessed non-uniformly along the DW length (shown in Fig. 5(c)), and all DWs quickly (<1 ns) evolved into non-homogeneously magnetized DWs independently of the initial state. Homogeneous Bloch-up and Bloch-down DWs were tried in order to look for systematic automotion-type displacements [35] in which, as stressed by Eqs. (1), the DW velocity depends on the DW magnetization angle. As the experimental pulses are extremely long in comparison with the typical DW magnetization motion times (be it precession or even relaxation), such a dependence is not to be expected. However, in the presence of disorder and for the long DWs considered, that are beyond the 1D physics leading to Eqs. (1), this has to be numerically tested.

We observe that the progression of the DW position is noisy as a consequence of the precessions induced by the random variation of material parameters. To illustrate this, we have repeated 30 simulations with different random grains and three different DW initial states (Bloch wall pointing up, down and randomized), for $J=2.5\times10^{11}$ A/m^2 and $\mu_0Hz = 25$ mT. Figure 5(a) shows the typical dispersion of DW position with time. Although the DW velocity varies randomly, we observe that the mean velocity is linearly dependent on the applied current. In the inset of Fig. 5(a), we show the progression of a DW for different current densities (under $\mu_0Hz =25$ mT). The random fluctuation of the DW position qualitatively matches the experimental results shown above. Quantitatively, however, the DW position fluctuations are smaller than seen in experiments and, more importantly, the zero average DW displacement is obtained only in a restricted vicinity of the current, when it compensates the applied field effect. It is possible that this discrepancy simply stems from the simplicity of the disorder model used here, but this requires a systematic simulation study that is beyond the scope of this experimental paper.

To conclude, we have experimentally investigated the combined effect of field and current on DW motion in epitaxial [Co/Ni] samples with strong perpendicular anisotropy, in micro-wire devices and using Kerr microscopy. A strong impact of both amplitude and polarity of current on DW propagation, in two different velocity regimes, has been observed. The experimental data may be explained by the presence of both non-adiabatic and adiabatic terms in the STT expression. In the flow regime, the behavior of DW velocity is consistent with the 1D model. At high currents, when opposing the field effect, a stochastic behavior is observed for the first time. Real-scale 2D micromagnetic simulations show a random fluctuation of the DW position that qualitatively matches the experimental results. Surprisingly, this stochasticity experimentally extends over a large field and current range.

REFERENCES :

[1] J. Slonczewski, J. Magn. Magn. Mater. **159**, L1 (1996)

[2] L. Berger, Phys. Rev. B **54**, 9353 (1996)

[3] S. S. P.Parkin, M. Hayashi, L. Thomas, Science **320**, 190 (2008)

[4] M. Hayashi, L. Thomas, R. Moriya, C. Rettner, S. S. P.Parkin, Science **320**, 209 (2008)

[5] S. Mangin, D. Ravelosona, J. A. Katine, M. J. Carey, B. D. Terris, and E. E. Fullerton, Nat. Mater. **5**, 210 (2006)

[6] S. Le Gall, J. Cucchiara, M. Gottwald, C. Berthelot, and C.-H. Lambert, Y. Henry, D. Bedau, D. B. Gopman, H. Liu, A. D. Kent, J. Z. Sun, W. Lin, D. Ravelosona, J. A. Katine, E. E. Fullerton, and S. Mangin, Phys. Rev. B **86**, 014419 (2012)

[7] D. Ravelosona, S. Mangin, J. A. Katine, E. E. Fullerton, B. D. Terris, Appl. Phys. Lett. **90**, 072508 (2006)

[8] G. Chen, T. Ma, A. T. N'Diaye, H. Kwon, C. Won, Y. Wu, & A. K. Schmid, Nature Comm. **4**, 2671 (2013)

[9] S. M. Mohseni, S. R. Sani, J. Persson, T. N. Anh Nguyen, S. Chung, Ye. Pogoryelov, P. K. Muduli, E. Iacocca, A. Eklund, R. K. Dumas, S. Bonetti, A. Deac, M. Hoefer, and J. Åkerman, Science **339**, 1295 (2013)

[10] K-S. Ryu, S-H. Yang, L. Thomas and S. S. P. Parkin, Nature Comm. **5**, 3910 (2014)

[11] C. Burrowes, A. P. Mihai, D. Ravelosona, J.-V. Kim, C. Chappert, L. Vila, A. Marty, Y. Samson, F. Garcia-Sanchez, L. D. Buda-Prejbeanu, I. Tudosa, E. E. Fullerton and J.-P. Attané, Nature Phys. **6**, 17 (2010)

[12] T. Koyama, D. Chiba, K. Ueda, K. Kondou, H. Tanigawa, S. Fukami, T. Suzuki, N. Ohshima, N. Ishiwata, Y. Nakatani, K. Kobayashi and T. Ono, Nature Mater. **10**, 194 (2011)

[13] S. Girod, M. Gottwald, S. Andrieu, S. Mangin, J. McCord, Eric E. Fullerton, J-M. Beaujour, B. J. Krishnatreya and A. D. Kent, Appl. Phys. Lett. **94**, 262504 (2009)

[14] M. Gottwald, S. Girod, S. Andrieu, S. Mangin, Mat. Sci. Engin. **12**, 012018 (2010)

[15] S. Le Gall, N. Vernier, F. Montaigne, M. Gottwald, D. Lacour, M. Hehn, D. Ravelosona, S. Mangin, S. Andrieu and T. Hauet, Appl. Phys. Lett. **106**, 062406 (2015)

[16] A. Thiaville, Y. Nakatani, J. Miltat and Y. Suzuki, Europhys. Lett. **69**, 990 (2005)

[17] G. Tatara and H. Kohno, Phys. Rev. Lett. **92**, 086601 (2004)

[18] G. Tatara, H. Kohno, J. Shibata, Phys. Rep. **468**, 213-301 (2008)

[19] T. Koyama, K. Ueda, K.-J. Kim, Y. Yoshimura, D. Chiba, K. Yamada, J.-P. Jamet, A. Mougin, A. Thiaville, S. Mizukami, S. Fukami, N. Ishiwata, Y. Nakatani, H. Kohno, K. Kobayashi & T. Ono, Nature Nanotech. **7**, 635 (2012)

[20] I. M. Miron, K. Garello, G. Gaudin, P-J. Zermatten, M. V. Costache, S. Auffret, S. Banbiera, B. Rodmacq, A. Schuhl and P. Gambardella, Nature **476**, 189 (2011)

[21] K-S. Ryu, L. Thomas, S-H. Yang and S. S. P. Parkin, Nature Nanotech. **8**, 527 (2013)

[22] A. Kirilyuk, J. Ferré, V. Grolier, J-P. Jamet, D. Renard, J. Magn. Magn. Mater. **171**, 45 (1997)

[23] K. Yamada, J-P. Jamet, Y. Nakatani, A. Mougin, A. Thiaville, T. Ono, and J. Ferré, App. Phys. Express **4**, 113001 (2011)

[24] T. Koyama, D. Chiba, K. Ueda, H. Tanigawa, S. Fukami, T. Suzuki, N. Ohshima, N. Ishiwata, Y. Nakatani, and T. Ono, Appl. Phys. Lett. **98**, 192509 (2011)

[25] J. Ryu, S-B. Choe and H-W Lee, Phys. Rev. B **84**, 075469 (2011)

[26] O. Boulle, J. Kimling, P. Warnicke, M. Klaüi, and U. Rüdiger, G. Malinowski, H. J. M. Swagten, and B. Koopmans, C. Ulysse and G. Faini, Phys. Rev. Lett. **101**, 216601 (2008)

[27] J-C. Lee, K-J. Kim, J. Ryu, K-W. Moon, S-J. Yun, G-H. Gim, K-S. Lee, K-H. Shin, H-W. Lee and S-B. Choe, Phys. Rev. Lett. **107**, 067201 (2001)

[28] K-J. Kim, J-C. Lee, K-H. Shin, H-W. Lee and S-B. Choe, Curr. Appl. Phys. **13**, 228-236 (2013)

[29] DW thickness is estimated as $\Delta=(A/K_{eff})^{\frac{1}{2}}$ with A= 10×10^{-12} J/m the exchange constant for Co/Ni.

[30] J. Curiale, A. Lemaître, G. Faini and V. Jeudy, Appl. Phys. Lett. **97**, 243505 (2010)

[31] J-M. L. Beaujour, W. Chen, K. Krycka, C-C. Kao, J. Z. Sun, and A. D. Kent, Eur. Phys. J. **59**, 475-483 (2007)

[32] T. Hauet, M. Gottwald, A. Neggache, A. Rajanikanth, F. Montaigne, S. Mangin, F. Bertran, P. Le Fèvre, F. Gimbert, L. Calmels, S . Andrieu, in preparation (2016)

[33] K. Ueda, T. Koyama, R. Hiramatsu, D. Chiba, S. Fukami, H. Tanigawa, T. Suzuki, N. Ohshima, N. Ishiwata, Y. Nakatani, K. Kobayashi & T. Ono, Appl. Phys. Lett. **100**, 202407 (2012)

[34] H. Tanigawa, T. Suzuki, S. Fukami, K. Suemitsu, N. Ohshima, and E. Kariyada, Appl. Phys. Lett. **102**, 152410 (2013)

[35] J-Y. Chauleau, R. Weil, A. Thiaville, and J. Miltat, Phys. Rev. B **82**, 214414 (2010)

[36] L. Thomas, R. Moriya, C. Rettner, S.S.P. Parkin, Science **330**, 1810 (2010)

[37] S. Fukami, M. Yamanouchi, S. Ikeda and H. Ohno, Nat. Commun. **4**, 2293 (2013)

[38] A Vansteenkiste, J Leliaert, M Dvornik, M Helsen, F Garcia-Sanchez and B Van Waeyenberge, AIP Advances **4**, 107133 (2014)
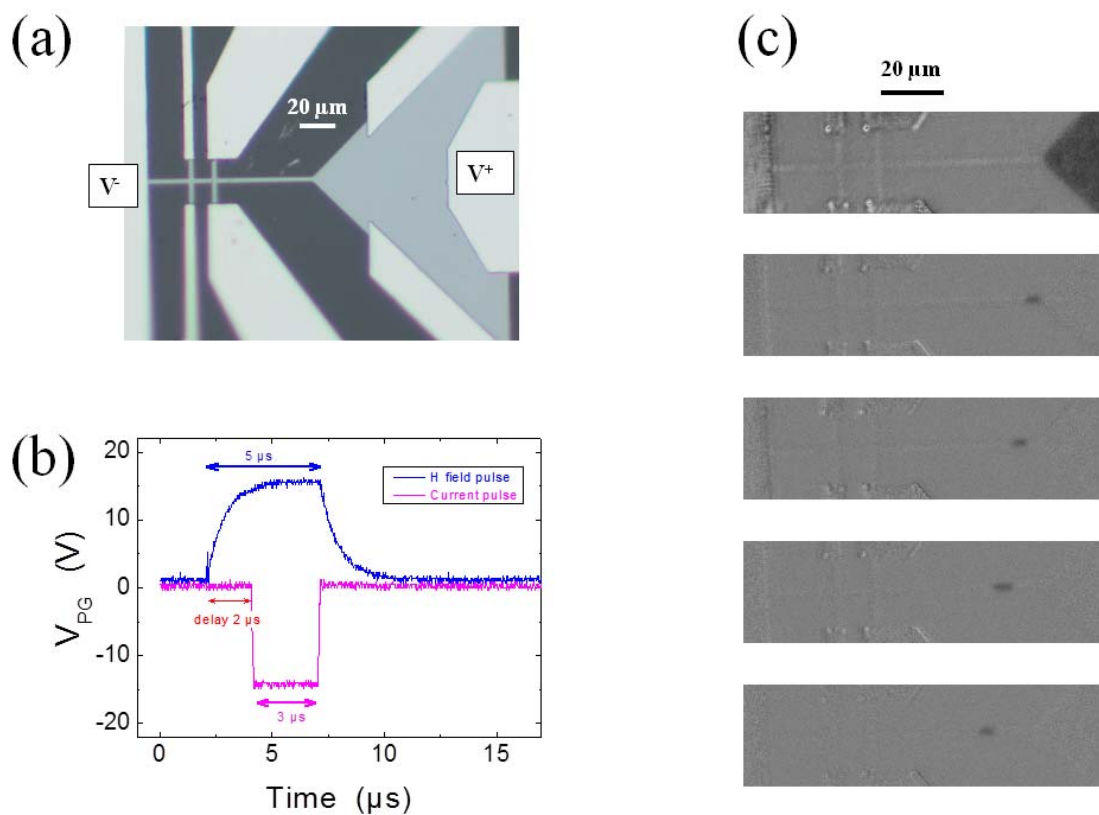
FIG. 1 : (a) Optical picture of a typical 2 µm wide wire studied here, with electrical connections. (b) Pulse synchronization for H field (blue) and current (magenta): duration is 5 µs for H_{pulse}, 3 µs for I_{pulse} with a delay of 2 µs. The current and field amplitudes can be tuned for each pulse with the following calibration: V_{PG} =14.6 V amplitude for $\mu_0 H_{pulse}$ corresponds to 12.75 mT and V_{PG} = -15 V for I_{pulse} corresponds to a current of 9.68 mA. (c) Example of DW displacement sequence on a 2 µm wire width for J_{pulse}=+21×10^{10} A/m² and $\mu_0 H_{pulse}$=20.5 mT. The black magnetic contrast corresponds to the DW displacement in the field direction during 1 pulse (difference of 2 pictures, taken at zero field before and after the pulse).
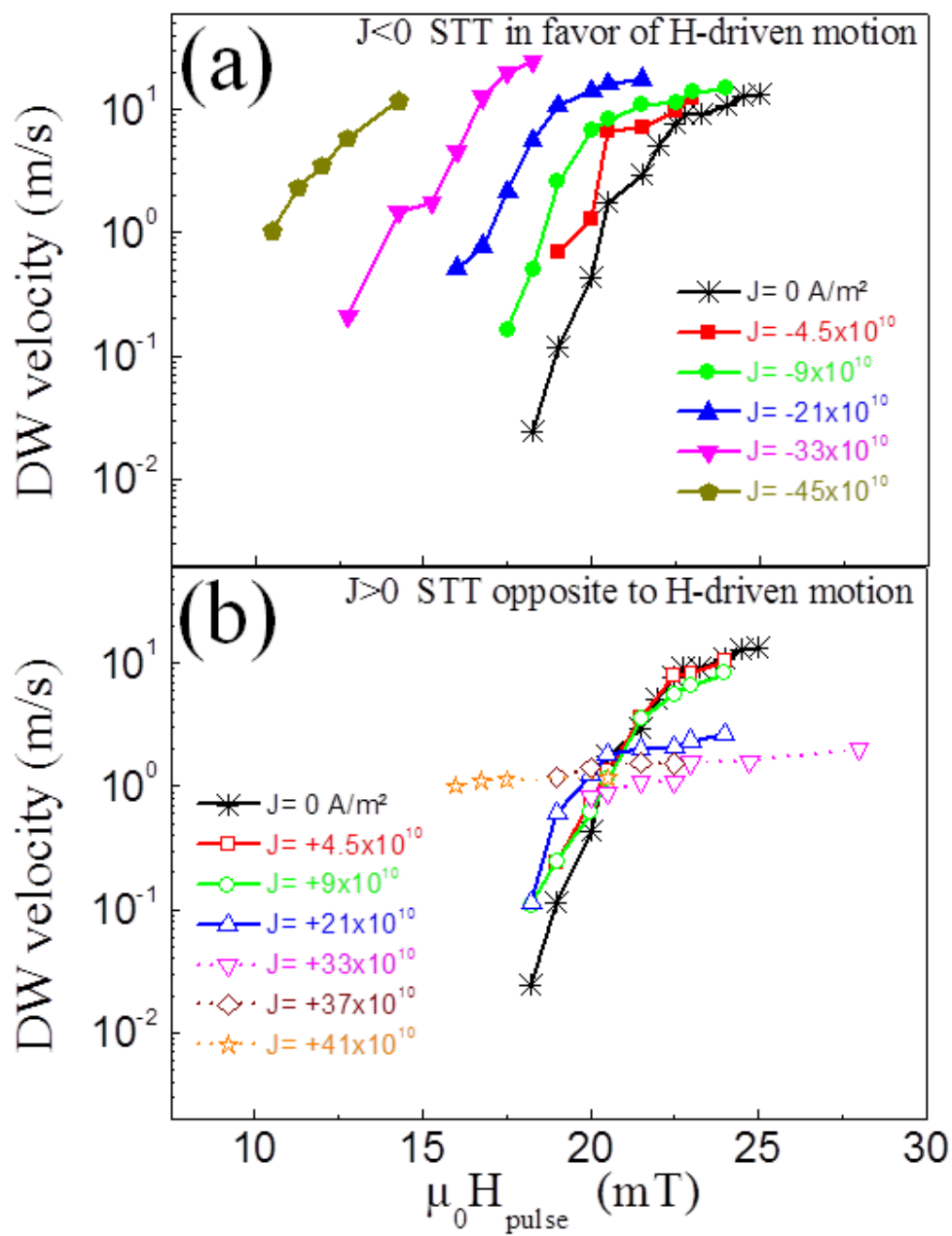
(a) J<0 STT in favor of H-driven motion

J= 0 A/m²
J= -4.5×10¹⁰
J= -9×10¹⁰
J= -21×10¹⁰
J= -33×10¹⁰
J= -45×10¹⁰

(b) J>0 STT opposite to H-driven motion

J= 0 A/m²
J= +4.5×10¹⁰
J= +9×10¹⁰
J= +21×10¹⁰
J= +33×10¹⁰
J= +37×10¹⁰
J= +41×10¹⁰

DW velocity (m/s)

$\mu_0 H_{pulse}$ (mT)

FIG. 2 : Combined field and current-driven DW motion in a wire having a 2 μm width. (a) DW velocity as a function of $\mu_0 H_{pulse}$ in semi-logarithmic scale for various (a) negative J_{pulse} (full symbols) and (b) positive J_{pulse} (open symbols). Note that the curves for $J_{pulse} \geq 33 \times 10^{10}$ A.m^{-2} are in dotted lines because they correspond to a specific regime discussed at the end of the paper.
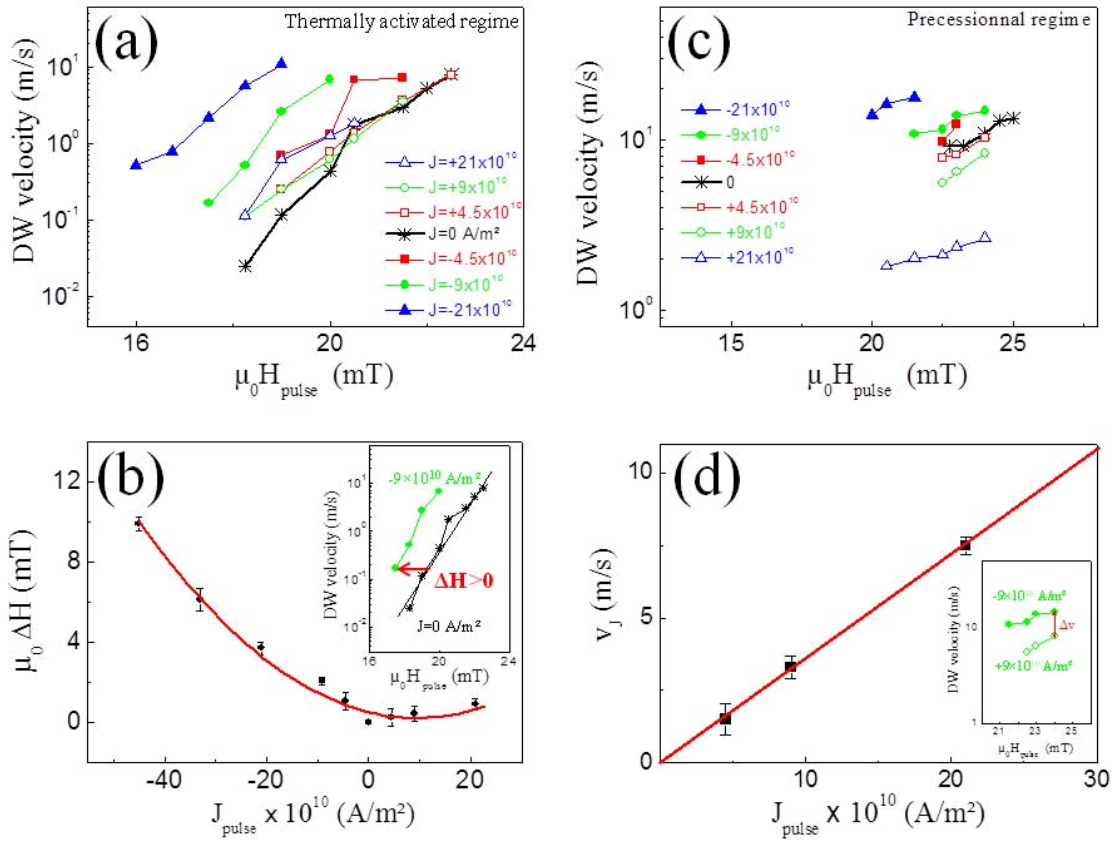

FIG. 3 : DW velocities, restricted to the thermally-activated regime (a)&(b) and to the precessional flow (c)&(d). (a) DW velocity *versus* $\mu_0 H_{pulse}$ for various J_{pulse} in the thermally-activated regime. (b) $\mu_0 \Delta H$ *versus* J_{pulse} in order to extract ε and η parameters. The ΔH is a mean of the field shift for each velocity at Jpulse≠0. The black symbols are experimental data and the red line is a polynomial fit. The error bars are given by the standard deviation from the determination of ΔH. Inset of (b) : example of

field shift determination for $\mu_0 H = 17.5$ mT for the velocity at $J = -9 \times 10^{10}$ A/m². (c) DW velocity *versus* $\mu_0 H_{pulse}$ for various J_{pulse} in the precessional flow regime. (d) Plot of v_J *versus* J_{pulse}; the inset depicting the method for extracting Δv where the mean gives $2 \times v_J$ (for instance Δv is displayed for $J_{pulse} = +/- 9 \times 10^{10}$ A/m² at $\mu_0 H = 24$ mT). The red line is a linear fit and the error bars are the standard deviation from the determination of v_J.
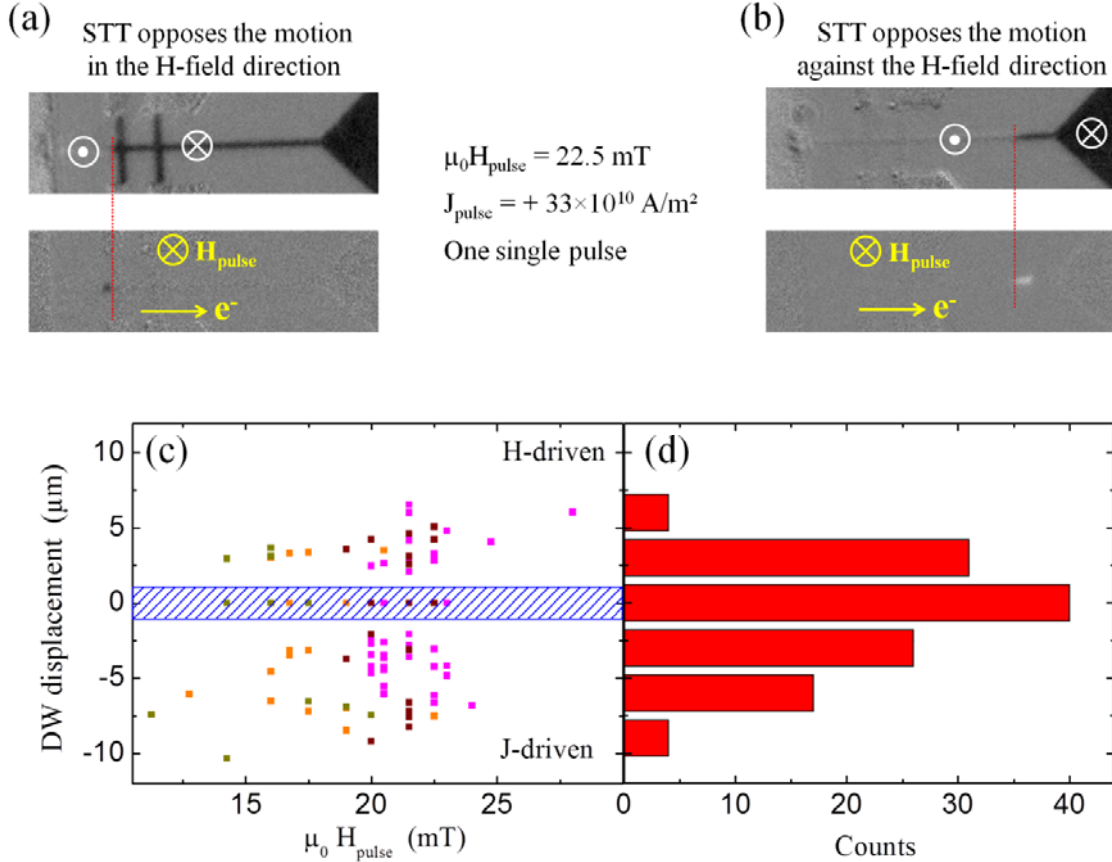

FIG. 4 : STT effect on DW motion for strong $J_{pulse} > 33 \times 10^{10}$ A/m². (a) and (b) are DW displacement observations for combined $\mu_0 H_{pulse} = 22.5$ mT and $J_{pulse} = +33 \times 10^{10}$ A/m² excitations, which lead to movements in 2 opposite directions. Cases (a) and (b) are called respectively H-driven and J-driven. Each case is depicted by 2 MOKE pictures: the upper one represent the DW position in the wire before pulses with magnetic states of each domain shown (white symbols); the bottom one is the DW position after the combined H_{pulse} and J_{pulse} excitations (both displayed in yellow). The black magnetic contrast corresponds to the H-driven DW motion, the white one to the J-driven case. (c) Plot of all experimental data points measured for DW displacement *versus* $\mu_0 H_{pulse}$ for various J_{pulse} (magenta: 33, brown: 37, orange: 41 and dark yellow: 45×10^{10} A/m²). Positive displacement is for H-driven, negative one for J-driven. The blue shaded region represents the range of DW pinning or auto-motion (points located in this region correspond to several measurements). (d) Bar graph of the DW displacement. The statistics was built from all experimental data from (c) without taking into account the value of the current.
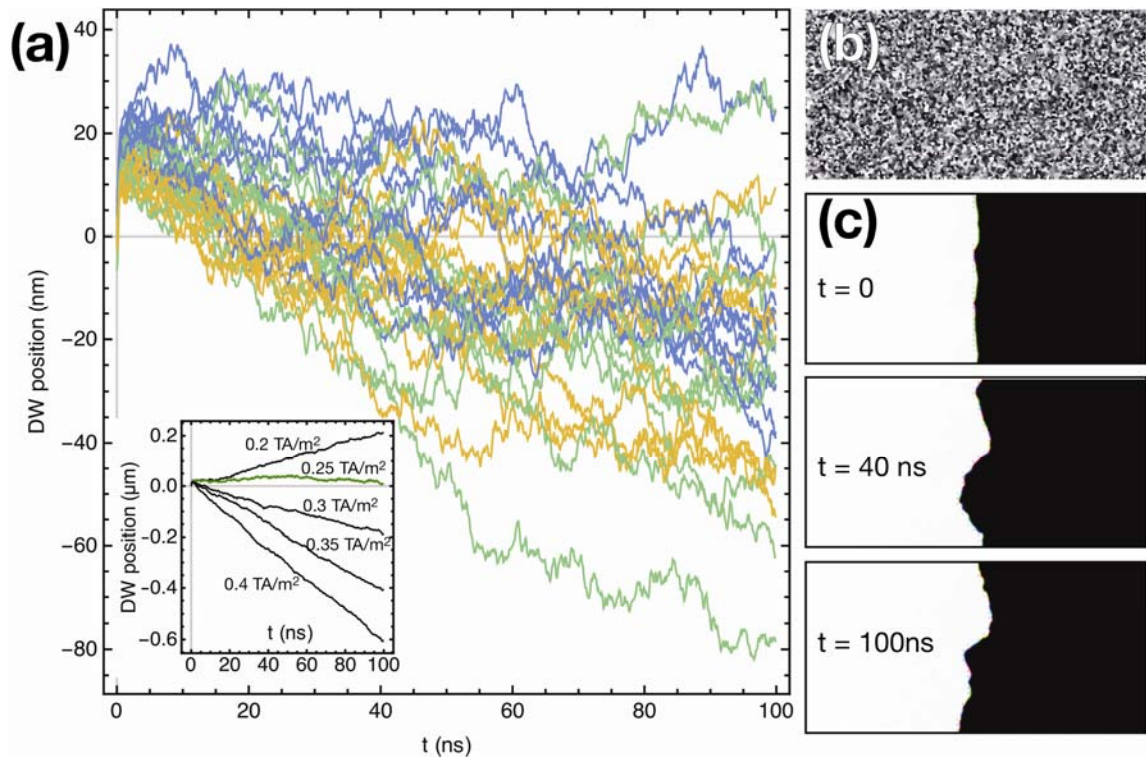
FIG. 5 : Micromagnetic simulations of DW propagation in an inhomogeneous film. (a) DW progression for 30 cases with different random grains and different DW initial states, for $\mu_0 Hz$=25 mT and J=2.5×10^{11} A/m^2. The colors correspond to the initial DW states (blue for Bloch up, green for Bloch down, and yellow for the randomized DW). The inset shows the progression for different current densities ($\mu_0 Hz$=25 mT). (b) Map of the random grains (the grayscale corresponds to the magnitude of M_S). (c) Three snapshots of the magnetisation corresponding to one of the curves in (a).